



Available online at [www.sciencedirect.com](http://www.sciencedirect.com)

ScienceDirect

journal homepage: [www.ejcancer.com](http://www.ejcancer.com)



## Original Research

# Comprehensive molecular and clinicopathological profiling of desmoid tumours



Shinji Kohsaka <sup>a,\*</sup>, Makoto Hirata <sup>b</sup>, Masachika Ikegami <sup>a</sup>,  
Toshihide Ueno <sup>a</sup>, Shinya Kojima <sup>a</sup>, Tomohisa Sakai <sup>c</sup>, Kan Ito <sup>c</sup>,  
Norifumi Naka <sup>d</sup>, Koichi Ogura <sup>e</sup>, Akira Kawai <sup>e</sup>, Shintaro Iwata <sup>e,f</sup>,  
Tomotake Okuma <sup>g</sup>, Tsukasa Yonemoto <sup>f</sup>, Hiroshi Kobayashi <sup>h</sup>,  
Yoshiyuki Suehara <sup>i</sup>, Hiroaki Hiraga <sup>j</sup>, Teruya Kawamoto <sup>k</sup>, Toru Motoi <sup>l</sup>,  
Yoshinao Oda <sup>m</sup>, Daisuke Matsubara <sup>n</sup>, Koichi Matsuda <sup>b</sup>,  
Yoshihiro Nishida <sup>c,\*\*\*</sup>, Hiroyuki Mano <sup>a,\*\*</sup>

<sup>a</sup> Division of Cellular Signaling, National Cancer Center Research Institute, 5-1-1 Tsukiji, Chuo-ku, Tokyo, 104-0045, Japan

<sup>b</sup> Laboratory of Genome Technology, Human Genome Center, Institute of Medical Science, The University of Tokyo, Tokyo, 108-8639, Japan

<sup>c</sup> Department of Orthopaedic Surgery, Nagoya University Hospital, Nagoya, 466-8550, Japan

<sup>d</sup> Musculoskeletal Oncology Service, Osaka International Cancer Institute, Osaka, 541-8567, Japan

<sup>e</sup> Department of Musculoskeletal Oncology, National Cancer Center Hospital, 5-1-1 Tsukiji, Chuo-ku, Tokyo, 104-0045, Japan

<sup>f</sup> Division of Orthopaedic Surgery, Chiba Cancer Center, Chiba, 260-8717, Japan

<sup>g</sup> Department of Musculoskeletal Oncology, Tokyo Metropolitan Cancer and Infectious Diseases Center Komagome Hospital, Tokyo, 113-0021, Japan

<sup>h</sup> Department of Orthopaedic Surgery, Faculty of Medicine, The University of Tokyo, Tokyo, 113-0033, Japan

<sup>i</sup> Department of Orthopedic Surgery, Juntendo University, Graduate School of Medicine, Tokyo, 113-8431, Japan

<sup>j</sup> Department of Orthopaedic Surgery, Hokkaido Cancer Center, Sapporo, 003-0804, Japan

<sup>k</sup> Department of Orthopaedic Surgery, Kobe University Graduate School of Medicine, Kobe, 650-0017, Japan

<sup>l</sup> Department of Pathology, Tokyo Metropolitan Cancer and Infectious Diseases Center Komagome Hospital, Tokyo, 113-0021, Japan

<sup>m</sup> Department of Anatomic Pathology, Graduate School of Medical Sciences, Kyushu University, 3-1-1 Maidashi, Higashi-ku, Fukuoka, 812-8582, Japan

<sup>n</sup> Division of Integrative Pathology, Jichi Medical University, Shimotsuke, 329-0498, Japan

Received 28 November 2020; accepted 2 December 2020

Available online 11 January 2021

\* Corresponding author: Division of Cellular Signaling, National Cancer Center Research Institute, 5-1-1 Tsukiji, Chuo-ku, Tokyo, 104-0045, Japan. Fax: +81 35565 0727.

\*\* Corresponding author: Division of Cellular Signaling, National Cancer Center Research Institute, 5-1-1 Tsukiji, Chuo-ku, Tokyo, 104-0045, Japan. Fax: +81 33248 0326.

\*\*\* Corresponding author: Department of Orthopaedic Surgery, Nagoya University Hospital, Tsurumai 65, Showa-ku, Nagoya, 466-8550, Japan. Fax: +81 52 744 2260.

E-mail address: [skohsaka@ncc.go.jp](mailto:skohsaka@ncc.go.jp) (S. Kohsaka), [ynishida@med.nagoya-u.ac.jp](mailto:ynishida@med.nagoya-u.ac.jp) (Y. Nishida), [hmano@ncc.go.jp](mailto:hmano@ncc.go.jp) (H. Mano).

<https://doi.org/10.1016/j.ejca.2020.12.001>

0959-8049/© 2020 The Author(s). Published by Elsevier Ltd. This is an open access article under the CC BY-NC-ND license (<http://creativecommons.org/licenses/by-nc-nd/4.0/>).

**KEYWORDS**

Molecular profiling;  
Driver mutation;  
RNA-seq;  
Desmoid tumours

**Abstract** Previous studies have not clearly identified a prognostic factor for desmoid tumours (DT). Whole-exome sequencing (WES) and/or RNA sequencing (RNA-seq) were performed in 64 cases of DT to investigate the molecular profiles in combination with the clinicopathological characteristics. *CTNNB1* mutations with specific hotspots were identified in 56 cases (87.5%). A copy number loss in chromosome 6 (chr6) was identified in 14 cases (21.9%). Clustering based on the mRNA expression profiles was predictive of the patients' prognoses. The risk score generated by the expression of a three-gene set (*IFI6*, *LGMN*, and *CKLF*) was a strong prognostic marker for recurrence-free survival (RFS) in our cohort. In risk groups stratified by the expression of *IFI6*, the hazard ratio for recurrence-free survival in the high-risk group relative to the low-risk group was 12.12 (95% confidence interval: 1.56–94.2;  $p = 8.0 \times 10^{-6}$ ). In conclusion, *CTNNB1* mutations and a chr6 copy number loss are likely the causative mutations underlying the tumorigenesis of DT while the gene expression profiles may help to differentiate patients who would be good candidates for wait-and-see management and those who might benefit from additional systemic or radiation therapies.

© 2020 The Author(s). Published by Elsevier Ltd. This is an open access article under the CC BY-NC-ND license (<http://creativecommons.org/licenses/by-nc-nd/4.0/>).

## 1. Introduction

Desmoid tumours (DTs), which are also described as aggressive fibromatosis, are rare and locally aggressive neoplasms that arise from connective tissues (IARC WHO). The estimated annual incidence of DT is 5–6 cases per 1 million people, and this disease has a peak age of 30–40 years and a female predominance [1]. The common primary sites affected by DTs include the abdominal wall, mesentery, and extremities, and the lesions are occasionally close to the neurovascular bundle. Most DTs are sporadic (>90%) and harbour *CTNNB1* mutations, whereas a minority of tumours are associated with sporadic or hereditary *APC* mutations (i.e., Gardner's syndrome) [2–4].

Although DT is defined as an intermediate soft tissue tumour that lacks metastatic potential, these tumours may have varied and unpredictable natural histories, including spontaneous regression in up to 20% of patients [5]. Surgery is considered the standard of care for the primary treatment of DT; however, the risk of local recurrence remains unacceptably high (>40%) [6–8]. In recent years, patient surveillance, also known as the 'wait-and-see' approach, has been proposed as an option for initial management and an alternative to mutilating surgery [9,10].

Radiation therapy or systemic treatments are usually indicated in patients with progressive disease, a high risk of bowel obstruction or perforation, or disease-related symptoms such as severe pain, swelling, deformity, a loss of range of motion, or compromised vital organs. Systemic treatment options include non-steroidal anti-inflammatory drugs (NSAIDs), hormonal blockade, cytotoxic chemotherapy, and tyrosine kinase inhibitors [11–17]. A recent phase 3 clinical trial demonstrated the

antitumour activity of sorafenib, a multi-kinase inhibitor, in DT patients [18]. Moreover, a randomised, open-label, multicenter, phase 2 study demonstrated the clinical activity of pazopanib, a multi-tyrosine kinase inhibitor, in DT patients [19].

Reports have described several prognostic factors of the clinical outcomes of surgically resected DT. These include the patient's age, tumour size, location, surgical margin, and *CTNNB1* mutational status [20–25].

However, the lack of a comprehensive understanding of the biology of DT makes it difficult for physicians to stratify patients who would derive benefits from surgery or systemic treatments. Therefore, we conducted comprehensive molecular profiling analyses based on whole-exome sequencing (WES) and RNA sequencing (RNA-seq) and analysed those data in combination with the detailed clinical features of DT patients to identify biomarkers predictive of the prognosis of patients after surgery or drug treatments.

## 2. Materials and methods

### 2.1. Study design and patient specimens

The study cohort comprised 68 patients with DT who underwent surgical resection at hospitals participating in the Japan Sarcoma Genome Consortium, including Nagoya University Hospital, Osaka International Cancer Institute, National Cancer Center Hospital, Chiba Cancer Center, The University of Tokyo Hospital, Juntendo University Hospital, Tokyo Metropolitan Cancer and Infectious Diseases Center Komagome Hospital, Hokkaido Cancer Center, and Kobe University Hospital, between 2006 and 2016. A board-certified pathologist (TM) who specialized in sarcoma reviewed

the histological features of the DTs with reference to the criteria of the current World Health Organization classification. Fresh-frozen tumour samples were obtained from all patients. The study protocol was approved by the Ethics Committee of each participating institution. Written informed consent was obtained from all participants except those we were unable to contact due to a loss to follow-up or death at registration. For these latter cases, the Institutional Review Board at each participating institution granted permission for the use of existing tissue samples for research purposes. None of the samples used in this study were obtained from patients who had opted out of study participation.

## 2.2. Whole-exome sequencing, including mutation calls, copy number analysis, and signature analysis

Genomic DNA was isolated from fresh-frozen samples using the QIAamp DNA Mini Kit (Qiagen, Hilden, Germany), and 500 ng of each sample were subjected to target fragment enrichment using an Agilent Exome Kit (v6; Agilent Technologies, Santa Clara, CA, USA). Massively parallel sequencing of the isolated fragments was performed using the paired-end option on a HiSeq2500 platform (Illumina, San Diego, CA, USA). Paired-end WES reads were independently aligned to the human reference genome (hg38) using BWA [26], Bowtie2 (<http://bowtie-bio.sourceforge.net/bowtie2/index.shtml>), and NovoAlign (<http://www.novocraft.com/products/novoalign/>). Somatic mutations were called using MuTect (<http://www.broadinstitute.org/cancer/cga/mutect>), SomaticIndelDetector (<http://www.broadinstitute.org/cancer/cga/node/87>), and VarScan (<http://varscan.sourceforge.net>). Mutations were discarded if at least one of the following criteria were met: (1) the read depth was <20 or the VAF was <0.1; (2) the mutation was supported by only one strand of the genome; or (3) the mutation was present in normal human genomes included in either the 1000 Genomes Project dataset (<http://www.internationalgenome.org/>) or our in-house database. Gene mutations were annotated using SnpEff (<http://snpeff.sourceforge.net>). The copy number status was analysed using our in-house pipeline, which determines the logR ratio (LRR) as follows: (1) SNP positions in a homozygous state ( $\text{VAF} \leq 0.05$  or  $\geq 0.95$ ) or heterozygous state ( $\text{VAF} 0.4\text{--}0.6$ ) in the genomes of respective normal samples were selected from the 1000 Genomes Project database; (2) normal and tumour read depths at the selected position were adjusted based on the GpC percentage of a 100-bp window flanking the position [27]; (3) the LRR was calculated as the  $\log_2(t_i/n_i)$ , where  $n_i$  and  $t_i$  represent the normal and tumour-adjusted depths at position  $i$ , respectively; and (4) each representative LRR was determined by the median of a moving window (1 Mb) centred at position  $i$ . The LRRs of the copy numbers of alleles,

the major allele, and the minor allele were determined for every region of the genome. The  $p$ -values for the gains or losses of respective genomic regions were determined from the LRRs using a permutation test (100,000 iterations) according to the algorithm used in GISTIC [28,29]. The  $Q$ -values were calculated from these  $p$ -values using the R package  $q$  value (<http://github.com/jdstorey/qvalue>). The mutational signatures were analysed using the Wellcome Trust Sanger Institute Mutational Signature Framework (<http://jp.mathworks.com/matlabcentral/fileexchange/38724-wtsi-mutationalsignature-framework>). The optimal number of signatures was determined in accordance with the signature stabilities and average Frobenius reconstruction errors.

## 2.3. Transcriptome sequencing, expression analysis, and detection of fusion genes and exon skipping

Total RNA was extracted from fresh-frozen samples using RNA-Bee (Tel-Test Inc., Gainesville, FL, USA), treated with DNase I (Thermo Fisher Scientific, Waltham, MA, USA) and subjected to poly(A)-RNA selection prior to cDNA synthesis. The library used for RNA-seq was prepared using a NEBNext Ultra Directional RNA Library Prep Kit (NEB, Ipswich, MA, USA), in accordance with the manufacturer's protocol. Sequencing was conducted from both ends of each cluster using a HiSeq 2500 or NextSeq platform (Illumina). RNA-seq was aligned to hg19 using TopHat (v2.0.9; <https://ccb.jhu.edu/software/tophat/index.shtml>). The expression level of each gene was calculated using Cufflinks (v2.1.1; <http://cole-trapnell-lab.github.io/cufflinks>), and gene fusions were detected using the deFuse pipeline (<https://bitbucket.org/dranew/defuse>). Exon skipping was analysed using an in-house pipeline as follows: (1) the RNA-seq reads were aligned to hg38 and the NCBI reference sequence (RefSeq) using the Burrows–Wheeler Aligner and Bowtie2; (2) skipped exons were detected from the mapped RefSeq data; (3) virtual transcriptome sequences were created dynamically; (4) RNA-seq reads were aligned to the candidate transcriptome sequences; and (5) exon skipping candidates were identified from reads with a breakpoint.

## 2.4. Signature generation and statistical analysis

The survival data for our cohort were collected at Jun-tendo University. The recurrence-free survival (RFS) duration was defined as the time interval between the date of the surgical intervention and the date of recurrence, death from any cause, or the last follow-up. Univariate analysis was performed to select the 14 genes whose expression was significantly correlated to post-surgical prognosis ( $p$ -value <0.0005). Subsequently, stepwise variable selection procedures for regression

analysis (R package, My.stepwise) were performed. During this process, the three-gene set (*IFI6*, *LGMN*, and *CKLF*) was selected because it comprised the largest number of genes with *p*-values <0.05. The selected genes were then fitted into a stepwise multivariate Cox regression analysis to assess the relative contribution of each gene to the predictions of survival in our cohort. Next, the estimated regression coefficients from a multivariate Cox regression analysis were used to calculate a prognostic risk score for predicting RFS, as follows:

$$\text{Risk score} = \sum_{i=1}^n \exp_i * \beta_i$$

where *n* represents the number of prognostic genes, *exp<sub>i</sub>* represents the expression level of prognostic gene *i*, and *β<sub>i</sub>* represents the regression coefficient of gene *i*.

In this study, all statistical analyses were performed using R software (version 3.5.1; <https://www.r-project.org/>) and the packages contained therein. The survival analysis and Cox regression analyses were performed using the “survival” (v2.44.1.1) package. RFS was analysed using the Kaplan–Meier method, and differences in the survival curves according to either the risk score or the driver mutation subtype were evaluated using the log-rank test. The GSEA was performed using Java GSEA software (v2.2.4; <http://software.broadinstitute.org/gsea/index.jsp>).

### 2.5. Real-time quantitative PCR

Total RNA was extracted from the tumour samples with RNA-Bee reagent (Tel-Test Inc.) following the manufacturer’s instructions. To minimise genomic DNA contamination, DNase I digestion was performed. The reverse transcription reaction was performed with SuperScript IV VILO reverse transcriptase (Thermo Fisher Scientific) using 100 ng of the total RNA from each sample. The obtained cDNAs were subsequently used for quantitative PCR with Power SYBR Green PCR Master Mix (Thermo Fisher Scientific) on the 7500HT Fast Real-Time PCR System (Thermo Fisher Scientific). The primers specific for *IFI6* exon 4 (5'-TGGTCTGCGATCCTGAATG-3') and exon 5 (5'-AGAGGTTCTGGGAGCTGCTG-3'); for *ACTB* exon 4 (5'-AGAGCTACGAGCTGCCTGAC-3') and for exon 5 (5'-AGCACTGTGTTGGCGTACAG-3') were used to cover all the major transcript variants. The threshold cycle (CT) was detected automatically. Expression levels of mRNA were estimated using the 2<sup>−ΔΔCT</sup> method. The relative *IFI6* expression levels were normalised to that of the housekeeping gene *ACTB*. Then, the expression data were further converted to ratios with the average value. Experiments were performed in technical triplicates.

### 2.6. Data availability

We have deposited the raw sequencing data in the Japanese Genotype-Phenotype Archive (<http://trace.ddbj.nig.ac.jp/jga>), which is hosted by the DNA Data Bank of Japan, under accession number J-DS000337-001.

## 3. Results

### 3.1. Mutational profile of desmoid tumour

Sixty-four cases of surgically resected DT were subjected to whole-exome sequencing (WES), of which 55 were also subjected to RNA-seq. Non-synonymous *CTNNB1* mutations were identified in 56 cases (87.5%). The most common *CTNNB1* hotspot in our cohort was p.T41A, which was observed in 30 cases, followed by p.S45F (18 cases), p.S45P (5 cases), and others (1 each of p.S45\_G48del, p.D32V, and p.H36P) (Table 1). To evaluate whether the *CTNNB1* mutation was trunk one, the variant allele frequency (VAF) of *CTNNB1* was compared to that of the highest VAF among all mutated genes in each case. In *CTNNB1* mutation-positive cases, the ratio of the *CTNNB1* VAF to the highest VAF was 0.86, suggesting that *CTNNB1* is a trunk mutation in DT (Fig. 1A). The difference in the highest VAF between *CTNNB1*-positive and -negative cases was not significant (55 for positive cases versus 8 for negative cases). The average tumour mutation burden was 1.2 mutations/Mb; this burden was relatively lower than those associated with other solid tumours, consistent with the findings of a previous study [30]. Through chromosome (chr) copy number variation analyses, we also identified frequent copy number losses in 6q (14 cases, 21.9%) and amplifications in chr8, chr15, and chr20 (Fig. 1B and C). Truncating *APC* mutations were observed in two *CTNNB1* mutation-negative cases. One patient had germline *APC* p.Asn1548fs mutation and somatic p.Thr1160fs mutation. The other patient had somatic *APC* p.Gln1230\* mutation without germline *APC* mutation or loss of heterozygosity at the *APC* locus. The former patient was provided genetic counselling and underwent colonoscopy.

We further analysed whole-exome sequencing (WES) data for the six cases whose *CTNNB1* and *APC* were wildtypes. Somatic mutations in genes associated with *CTNNB1* were identified; *NPHS1* (*NPHS1* Adhesion Molecule, Nephrin) was mutated in two cases (#09 and 27), and *ZNF408* (Zinc Finger Protein 408) was mutated in one case (#23) (Supplementary Table S1). *NPHS1* encodes a member of the immunoglobulin family of cell adhesion molecules that functions in the glomerular filtration barrier of the kidney. *NPHS1* is known to play a role in skeletal muscle formation through the regulation of myoblast fusion downstream of the WNT/β-catenin signalling pathway [31]. The protein encoded by

Table 1

Mutational status and clinical information of the 64 desmoid tumours.

<i>CTNNB1</i>	VAF	<i>APC</i> mutation	Chr6 loss	Somatic mutation #	Somatic mutation frequency (/Mb)	Anatomical site	Age at diagnosis	Gender
#01 WT	0	—	—	181	1.79	Head and neck	33	F
#02 p.T41A	42.9	—	+	201	2.04	Extremity	40	F
#03 p.S45F	19.4	—	—	123	1.24	Head and neck	28	F
#04 p.S45F	38.7	—	—	107	1.11	Abdominal wall	28	F
#05 p.S45F	58.6	—	+	199	1.97	Trunk	29	M
#06 p.T41A	29.3	—	—	146	1.47	Extremity	32	F
#07 p.T41A	34.5	—	+	154	1.54	Abdominal wall	38	F
#08 WT	0	—	+	108	1.1	Abdominal wall	36	F
#09 p.S45_G48del	31.5	—	+	182	1.85	Abdominal wall	30	F
#10 p.S45F	47.2	—	—	136	1.38	Head and neck	19	F
#11 p.T41A	29.6	—	+	135	1.37	Extremity	19	F
#12 p.S45F	16.4	—	—	129	1.3	Trunk	41	M
#13 p.S45P	33.3	—	—	142	1.43	Abdominal wall	26	F
#14 p.T41A	1 (3/293)	—	—	127	1.28	Abdominal wall	35	F
#15 p.S45F	31.1	—	—	195	1.97	Head and neck	74	F
#16 p.T41A	36.4	—	—	128	1.29	Trunk	38	F
#17 p.T41A	37.8	—	—	96	0.95	Head and neck	38	M
#18 p.T41A	46.1	—	—	119	1.2	Abdominal wall	35	F
#19 WT	0	—	—	96	0.96	Extremity	40	F
#20 p.S45F	0.9 (3/326)	—	—	93	0.93	Abdominal wall	19	M
#21 WT	0	—	—	161	1.63	Extremity	33	F
#22 WT	0	—	—	111	1.15	Trunk	39	F
#23 p.S45F	35	—	—	104	1.07	Abdominal wall	19	F
#24 WT	0	—	—	155	1.6	Trunk	61	M
#25 p.T41A	2.8 (6/217)	—	—	105	1.08	Extremity	76	F
#26 p.T41A	35.5	—	+	141	1.44	Abdominal wall	33	M
#27 p.T41A	16.6	—	—	132	1.38	Trunk	62	F
#28 WT	0	+	—	115	1.18	Trunk	17	F
#29 p.S45F	36	—	—	107	1.09	Extremity	13	M
#30 p.T41A	47.5	—	+	134	1.39	Trunk	34	F
#31 p.S45F	6.3	—	—	106	1.09	Trunk	60	F
#32 p.D32V	33.6	—	—	163	1.69	Abdominal wall	34	F
#33 p.S45P	44.8	—	+	154	1.64	Head and neck	37	M
#34 p.S45F	30.1	—	—	101	1.06	Extremity	56	F
#35 p.S45F	32.2	—	—	88	0.9	Extremity	15	F
#36 p.S45P	37.9	—	—	117	1.21	Head and neck	57	F
#37 p.T41A	37.3	—	—	108	1.13	Trunk	38	F
#38 p.S45F	32.2	—	—	113	1.17	Trunk	68	M
#39 WT	0	+	+	157	1.61	Trunk	15	F
#40 p.S45F	11.7	—	—	180	1.86	Trunk	37	M
#41 p.T41A	23	—	—	476	4.93	Extremity	56	M
#42 p.S45F	48.7	—	+	195	2.02	Trunk	61	M
#43 p.T41A	40.4	—	—	144	1.5	Trunk	30	F
#44 p.T41A	36.4	—	—	99	1.02	Trunk	58	M
#45 p.T41A	28.5	—	—	141	1.46	Trunk	54	F
#46 p.T41A	32.3	—	—	191	1.98	Trunk	51	M
#47 p.S45P	46.9	—	+	176	1.87	Extremity	35	F
#48 p.T41A	39.9	—	—	162	1.69	Abdominal wall	17	F
#49 p.S45F	16.9	—	—	135	1.41	Trunk	55	F
#50 p.S45F	22.7	—	—	139	1.47	Trunk	28	F
#51 p.T41A	17.1	—	—	186	1.98	Trunk	31	F
#52 p.T41A	39.8	—	—	NA	NA	NA	NA	NA
#53 p.T41A	46.8	—	—	81	0.81	Extremity	20	F
#54 p.S45F	35.3	—	+	181	1.83	Trunk	79	M
#55 p.T41A	21.2	—	—	121	1.23	Extremity	39	F
#56 p.T41A	48	—	—	153	1.56	Trunk	35	M
#57 p.T41A	36.9	—	—	132	1.35	Trunk	56	F
#58 p.S45P	40.7	—	—	153	1.54	Abdominal wall	33	F
#59 p.H36P	43.8	—	—	125	1.27	Abdominal wall	28	F
#60 p.T41A	28.3	—	+	24	0.33	Extremity	25	M
#61 p.T41A	36.2	—	—	115	1.17	Extremity	5	M
#62 p.T41A	6.2	—	—	140	1.43	Extremity	36	F

(continued on next page)



Table 1 (continued)

<i>CTNNB1</i>	VAF	<i>APC</i> mutation	Chr6 loss	Somatic mutation #	Somatic mutation frequency (/Mb)	Anatomical site	Age at diagnosis	Gender
#63 p.T41A	39.9	—	—	136	1.36	Abdominal wall	39	F
#64 p.T41A	39.8	—	—	133	1.36	Head and neck	70	F

VAF, variant allele frequency (mutation reads/total reads); F, female; M, male; NA, not available.

*ZNF408* contains ten tandem zinc fingers and an N-terminal SET domain. In adults, the encoded protein is expressed most highly in the retina. Consequently, defects in this gene have been associated with familial exudative vitreoretinopathy (FEVR), which is also caused by a germline *CTNNB1* mutation [32]. Nucleus staining of *CTNNB1* was observed in three cases (#01, 09, and 23) by immunohistochemistry (Supplementary Fig. S1).

### 3.2. Transcriptional profiles of DTs

To identify the gene expression profiles associated with specific clinicopathological features or gene mutational profiles, we conducted a k-means clustering analysis using RNA-seq data. Clustering based on the top 100 most variable genes allowed us to divide the cohort into three groups (Fig. 2A).

We merged the clinical information and mutational profiles with the gene expression data and performed Fisher's exact test to determine the factors related to either group in the left cluster (cluster 1), middle cluster (cluster 2), and right cluster (cluster 3). Cluster 3 was enriched for female patients ( $p = 2 \times 10^{-4}$ ) relative to clusters 1 and 2. There was no significant difference in recurrence-free survival (RFS) among the clusters (Fig. 2B).

A gene set enrichment analysis (GSEA) revealed that the MYOGENESIS gene set was enriched in cluster 1 relative to clusters 2 and 3 (Fig. 2C and Supplementary Table S2). The expression of several genes related to skeletal muscle markers, such as *MYH1*, *MYL1*, and *ACTA1*, was elevated specifically in cluster 1, suggesting that the tumours in this cluster were associated with muscle differentiation (Supplementary Table S3).

The GSEA revealed that the MYC\_TARGETS gene set was enriched in recurrent tumours (Supplementary Fig. S2 and Supplementary Table S2). Patients who

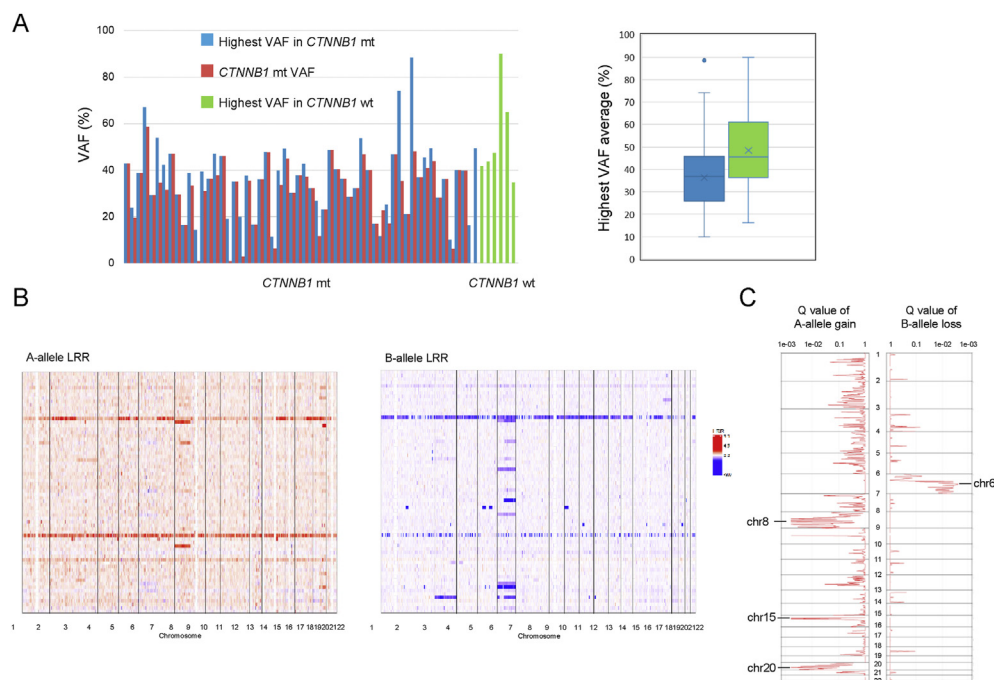


Fig. 1. Mutational profile of desmoid tumour. (A) The variant allele frequency (VAF) of *CTNNB1* was compared to that of the highest VAF found in each case (left panel). In *CTNNB1* mutation-positive cases, VAF ratio to the highest VAF was 0.86. The highest VAFs in 55 *CTNNB1*-mutant cases and 8 *CTNNB1*-wild type cases were compared (right panel). (B) Copy number change of major allele (left panel) or minor allele (right panel) throughout chromosome (horizontal axis) is shown by individual case (vertical axis). (C) The total profiles of allele-specific copy number alterations in desmoid tumour. Red lines indicate the Q-value for gains of major allele (left panel) and losses of minor allele (right panel). Chromosome numbers affected by copy number alteration are shown.

harboured *CTNNB1* p.S45F tended to have a worse prognosis than those harbouring other *CTNNB1* variants, although this difference was not statistically significant. The female sex ( $p = 6.7 \times 10^{-3}$ ) and lack of previous treatment ( $p = 4.2 \times 10^{-3}$ ) were identified as favourable factors in the survival analysis (Supplementary Fig. S3).

Patients with DT face a substantial risk of recurrence, even after complete surgical resection. Previous randomised trials of surgery have not demonstrated a consistent survival benefit. However, one case-control study revealed that the combination of surgery and radiotherapy yielded better local control than surgery alone [33]. There is a critical need for reliable prognostic biomarkers that can be used to select patients who face a high risk of recurrence, those who are good candidates for wait-and-see management, and those who might benefit from additional systemic or radiation therapies.

We analysed approximately 13,000 genes for which the expression profiles had large standard deviations (fragments per kilobase of exon per million mapped reads, FPKM >1.0) to ensure an adequate variance. A univariate Cox proportional hazards regression analysis revealed that 14 genes were significantly correlated with recurrence-free survival (RFS) ( $p \leq 5 \times 10^{-3}$ ), although

we note that genes that did not achieve significant correlations with RFS may also be important.

These 14 genes were used to build a prognostic signature in our cohort through a multivariable Cox analysis with a forward conditional stepwise regression. This procedure selected a prognostic model comprising three genes: *IFI6* (interferon alpha inducible protein 6), *LGMN* (legumain), and *CKLF* (chemokine like factor).

We constructed a risk score using the regression coefficients from this model and manually selected a suitable threshold at the 50th percentile (Fig. 3A). Patients in our cohort who were defined as high risk using this three-gene signature-based risk score had a significantly worse RFS ( $p = 2 \times 10^{-3}$ ; Fig. 3B). The median follow-up time for the low-risk group was 44 months, and that of the high-risk group was 35 months.

To understand the biology of high-risk tumours, we identified the top 100 significantly overexpressed and top 100 underexpressed genes in high-risk tumours (Fig. 3C and Supplementary Table S3). No clinical features were different between the low- and high-risk groups including *CTNNB1* p.S45, which was markedly but not significantly enriched in high-risk group ( $p = 0.18$ ). The gene sets related to cancer biology, such as EPIETHelial\_MESENCHYMAL\_TRANSITION,

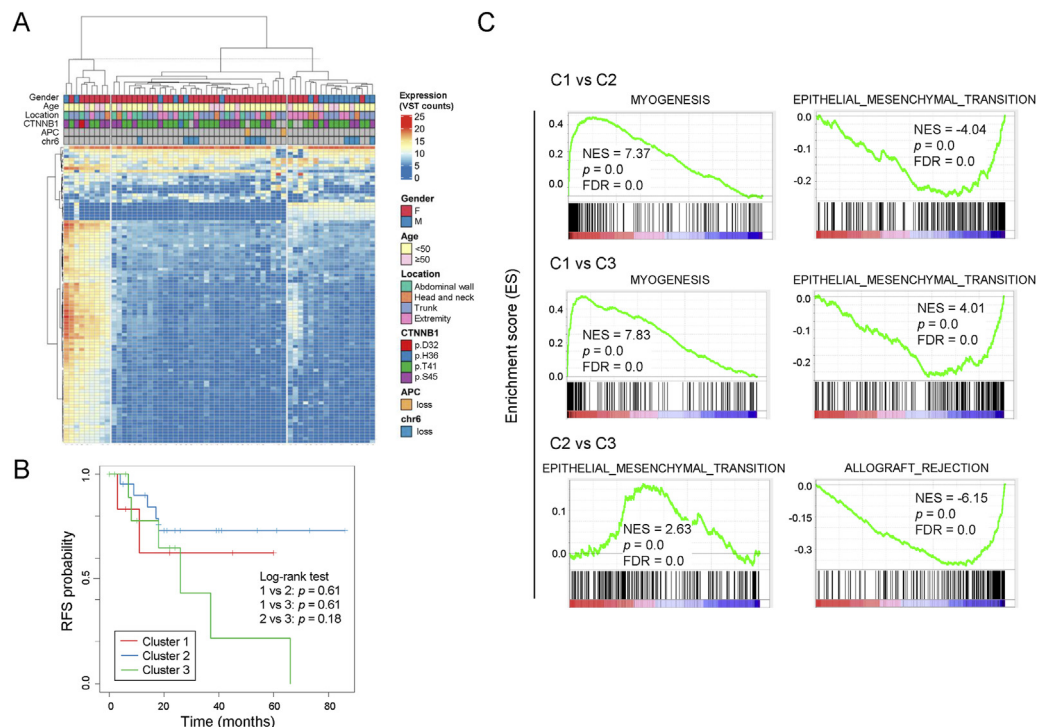


Fig. 2. Gene expression profile of desmoid tumour. (A) K-means clustering analysis was conducted using RNA-seq data. The clinical information (gender, age, location, mutational status, recurrence, and risk classification) are shown in the upper part. Fisher's test was performed to identify the factors associated with either group stratified by k-means clustering. (B) Kaplan–Meier curves of recurrence-free survival in our cohort stratified by k-means clustering as clusters 1 to 3. (C) GSEA results with the indicated gene sets among clusters defined by the k-means clustering are shown. Full GSEA results can be found in Supplementary Table S2.

were significantly enriched in the high-risk tumours, while the MYOGENESIS gene set was enriched in low-risk tumours (Fig. 3D and Supplementary Table S2).

Because *IFI6* was the only gene with a false discovery rate of  $\leq 0.05$ , we used the regression coefficients for *IFI6* expression to calculate a risk score and manually selected a suitable threshold at the 50th percentile (Fig. 4A). Patients in our cohort who were defined as high risk according to the *IFI6*-based risk score had a significantly worse RFS ( $p = 8 \times 10^{-6}$ ; Fig. 4B). The median follow-up time of the low-risk group was 36.5 months, and that of high-risk group was 48.5 months.

Real-time PCR of *IFI6* was performed to evaluate the concordance between assays. Although the expression value of real-time PCR was concordant with that of RNA-seq ( $r = 0.46$ ), the value of real-time PCR did not significantly stratify the patient prognosis after surgery ( $p = 0.13$ ) (Supplementary Fig. S4).

To understand the biology underlying high-risk tumours, we identified the top 100 significantly overexpressed and underexpressed genes in high-risk tumours

(Fig. 4C and Supplementary Table S3). No clinical features differed between the low- and high-risk groups. Significant enrichment of gene sets related to cancer biology, including EPITHELIAL\_MESENCHYMAL\_TRANSITION and INTERFERON\_ALPHA\_RESPONSE, was observed in the high-risk tumours, whereas the MYOGENESIS gene set was enriched in low-risk tumours (Fig. 4D and Supplementary Table S2).

Finally, a multivariable Cox analysis of our cohort revealed that the risk score remained statistically significant ( $HR = 11.7$ ,  $p = 0.02$ ) regardless of age, sex, tumour size, margin, location, previous surgical history, and gene mutations (Table 2). The previous surgical history was also a risk factor for recurrence ( $p = 0.04$ ). The tumour size and tumour location appeared to be prognostic factors, although the  $p$ -values of approximately 0.1 were likely attributable to the small cohort size. However, none of the mutation statuses were identified as statistically significant in the Cox analysis. There was no significant difference in the risk of recurrence between R0 (margin negative) and R1/2 (margin positive) cases.

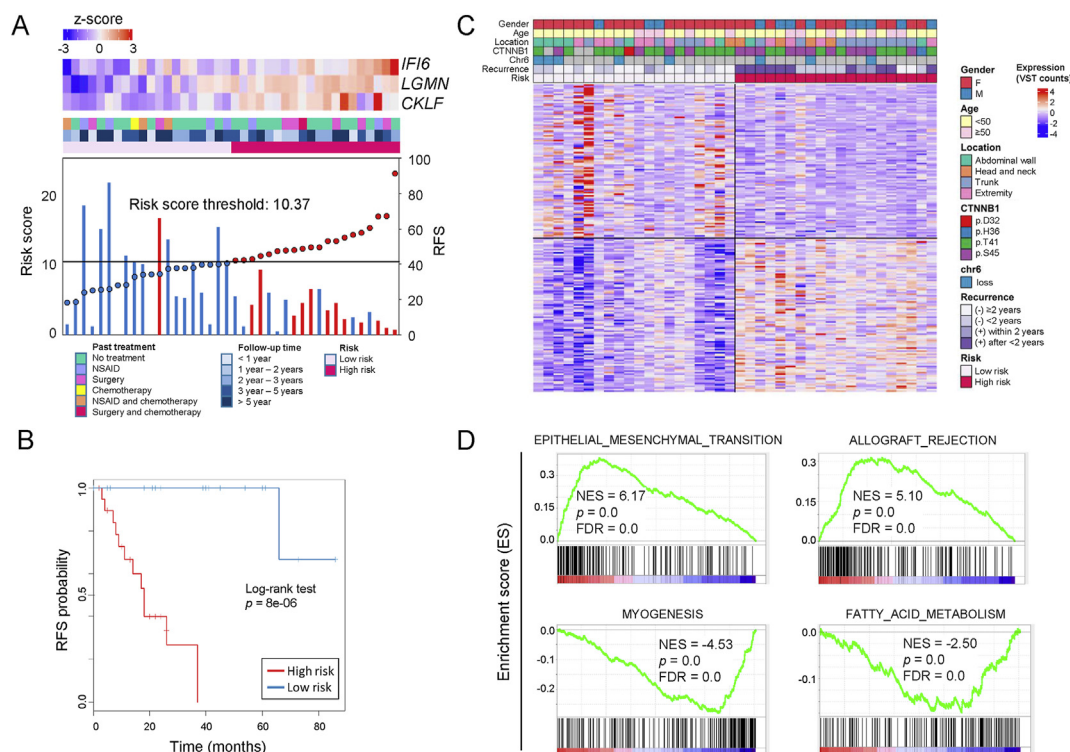


Fig. 3. Three-gene prognostic signature of DT. (A) Three-gene expression and risk score distribution in our cohort by z-score. Here, red indicates higher expression, while light blue indicates lower expression. The risk scores for all patients are plotted in ascending order and marked as low risk (blue) or high risk (red), as divided by the threshold (vertical black line). The risk score threshold is 10.4. The bars indicate the RFS times for each case. Red bars represent recurrent cases and blue bars represent no recurrence during observation. (B) Kaplan–Meier curves of recurrence-free survival in the cohort stratified by three-gene prognostic signature into those at high and low risk. Log-rank test was used to evaluate  $p$ -value. (C) Heatmap of the top 200 genes differentially expressed between those at high and low risk, with red indicating higher expression and blue indicating lower expression. (D) Statistically significant gene sets identified by GSEA to be differentially overexpressed in high-risk tumours. Supplementary Table S2 presents the full GSEA results. NES, normalised enrichment score; FDR, false discovery rate.



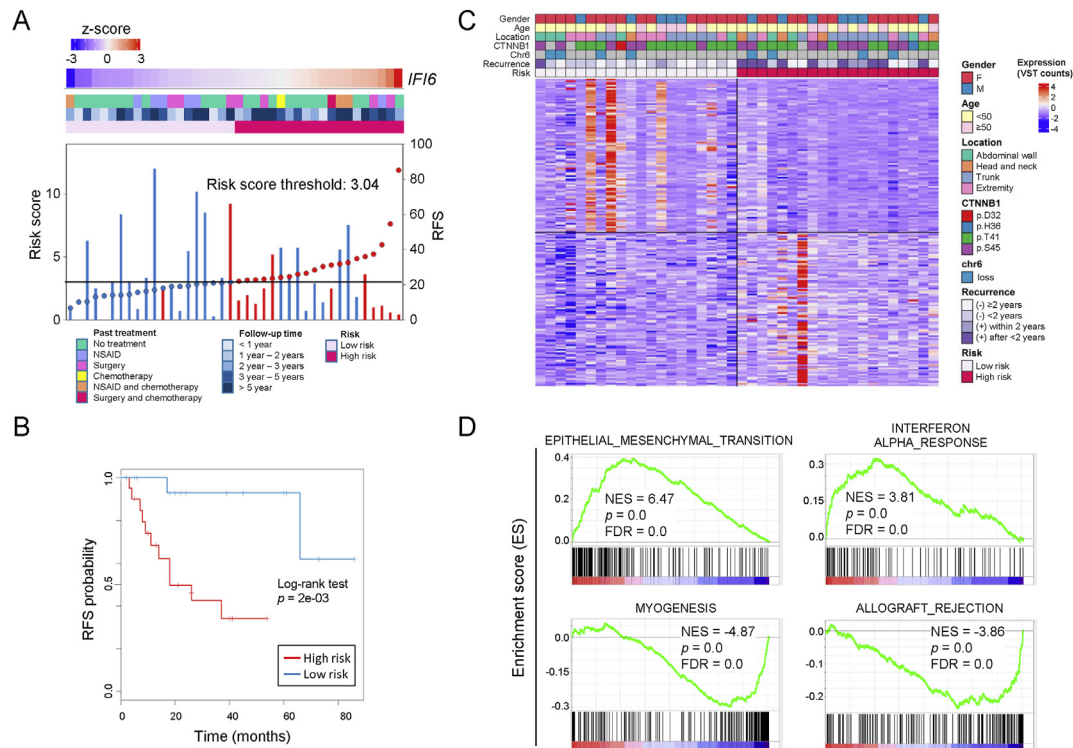


Fig. 4. *IFI6* expression as a prognostic signature of DT. (A) *IFI6* expression and risk score distribution in our cohort by z-score. Here, red indicates higher expression, while light blue indicates lower expression. The risk scores for all patients are plotted in ascending order and marked as low risk (blue) or high risk (red), as divided by the threshold (vertical black line). The risk score threshold is 3.0. The bars indicate the RFS times of each case. Red bars are recurrent cases, and blue bars represent no recurrence during the observation. (B) Kaplan–Meier curves of recurrence-free survival in the cohort stratified by *IFI6* prognostic signature into those at high and low risk. Log-rank test was used to evaluate  $p$ -value. (C) Heatmap of the top 200 genes differentially expressed between those at high and low risk, with red indicating higher expression and blue indicating lower expression. (D) Statistically significant gene sets identified by GSEA to be differentially overexpressed in high-risk tumors. [Supplementary Table S2](#) presents the full GSEA results. NES, normalised enrichment score; FDR, false discovery rate.

To investigate whether the risk score for RFS after surgery also correlated to the prognosis after treatments with NSAIDs, the risk scores and progression-free survival (PFS) were compared in 14 patients who were treated with NSAIDs as the first-line treatment. Neither risk classification by the three-gene set nor *IFI6* could stratify the PFS of the NSAIDs treatment ([Supplementary Fig. S5](#)).

#### 4. Discussion

Although DTs are frequently positive for mutations in *CTNNB1* or *APC*, six of 64 cases (9.4%) in our cohort were negative for both mutations. *CTNNB1* mutation is a trunk mutation and is therefore a likely genetic driver of DT growth. As we observed no difference in the highest VAF among gene mutations between *CTNNB1* mutation-positive and -negative cases, this suggests that the latter cases were true-negatives rather than false-negatives, due to low tumour content. A previous comprehensive genomic analysis of DT that targeted the exonic regions of 27 genes also identified *CTNNB1* mutations or *APC* germline mutations in approximately

90% of cases, but detected few other oncogenic mutations in *CTNNB1* wild-type DTs [4]. Further analyses based on other analytic modalities, such as long-read sequencing, may be important for deciphering the mechanism underlying the malignant transformation of *CTNNB1* wild-type DT.

The hierarchical clustering analysis identified a distinct cluster in which genes related to myogenesis, such as *MYH1*, *MYL1*, *ACTA1*, or *CKM*, were strongly expressed. We note that this cluster was not associated with any specific clinical features or with chr6 loss, suggesting that the latter factor may be associated with a myogenic differentiation block.

We defined a three-gene set that could predict the aggressive type of DT. This gene set might be a good predictive biomarker for differentiating patients who are good candidates for wait-and-see management and those who might benefit from additional systemic or radiation therapies. The three-year recurrence-free survival rate of the low-risk group after surgery was 100%, whereas that of high-risk group was 33%. Notably, the three-year recurrence-free survival rate of patients with a risk score >12 was 0%. Therefore,

Table 2

Cox proportional hazard models in desmoid tumour.

Variables	Categories	No.	Univariate analysis			Multivariate analysis		
			Hazard ratio	95% CI	*P value	Hazard ratio	95% CI	*P value
Gender	Female	28						
	Male	12	4.49	1.46–13.81	0.01	2.87	0.90–9.11	0.07
Age	<50	28						
	≥50	12	1.30	0.42–4.03	0.65			
Size	<10	24						
	≥10	14	2.93	0.86–10.05	0.09			
Margin	R0	15						
	R1, R2	21	1.01	0.28–3.61	0.99			
Location	Abdominal wall	8						
	Head and neck	5	10.15	0.85–121.19	0.07			
	Trunk	16	4.70	0.52–42.27	0.17			
	Extremity	11	5.50	0.61–49.76	0.13			
Surgical history	No	32						
	Yes	8	4.25	1.39–12.98	0.01	3.49	1.05–11.65	0.04
CTNNB1 mutation	T41	20						
	S45	15	1.82	0.61–5.44	0.28			
Chr6 loss	F	34						
	T	6	0.67	0.15–3.04	0.60			
Cluster	Cluster 1	6						
	Cluster 2	22	0.52	0.10–2.71	0.44			
	Cluster 3	12	1.54	0.31–7.76	0.60			
Risk score (3 genes)	Low risk	20						
	High risk	20	4E+09	0-Inf	1.00			
Risk score (IFI6)	Low risk	20						
	High risk	20	12.12	1.56–94.2	0.02	11.71	1.48–92.83	0.02

\*Two-sided likelihood ratio test. RFS, recurrence-free survival; CI, confidence interval; R0 – no cancer cells seen microscopically at the resection margin; R1 – cancer cells present microscopically at the resection margin (microscopic positive margin); R2 – gross examination by the naked eye shows tumour tissue present at the resection margin (macroscopic positive margin).

tumours with a high-risk score may need resection with an extra margin. Neither the risk classification by the three-gene set nor *IFI6* could stratify the prognosis after NSAIDs treatment, so tumours with a low-risk score may need to be resected if they do not respond to NSAIDs.

These three genes are related to apoptosis, invasion, or inflammation. *IFI6* negatively regulates the intrinsic apoptotic signalling pathway and TNF-induced apoptosis [34–36]. In breast cancer, the upregulation of *IFI6* was associated with a poor RFS [37] and poor distance metastasis-free survival [38], and this effect was probably mediated by enhanced breast cancer cell migration and invasion. *IFI6* was also reported to be necessary for *NRAS*-induced transformation and melanoma growth through its ability to reduce DNA replication stress [39].

*LGMN* encodes a cysteine protease that is strictly specific for the hydrolysis of asparaginyl bonds. Recent studies of human tumours have shown that the expression of *LGMN* correlates closely with a poor prognosis [40–42], as the product of this gene promotes the invasion and migration of tumour cells. tumour cell-derived LGMN and circulatory LGMN have prometastatic effects and have been reported as prognostic markers in breast cancer patients [43].

*CKLF* is a cytokine and potent chemoattractant for neutrophils, monocytes, and lymphocytes. This cytokine also can stimulate the proliferation of skeletal muscle cells and may play important roles in inflammation and skeletal muscle regeneration [44]. However, few previous studies have explored the association of *CKLF* with cancer.

Our GSEA identified an association of the high-risk group with mesenchymal features, as well as an association of the low-risk group with myogenic differentiation. The epithelial–mesenchymal transition (EMT) is a process by which epithelial cells lose their cell polarity and cell–cell adhesion properties and gain migratory and invasive properties; in other words, these cells become mesenchymal stem-like cells. The enrichment of a gene set related to EMT may indicate the high invasion and migration capabilities of aggressive DTs. Importantly, the upregulation of *IFI6* and *LMGN* may contribute to the survival and invasion of DT cells and thus may the association of these factors with a poor prognosis. The lack of genetic differences between the high-risk and low-risk tumours suggests that epigenetic changes may contribute to the progression and recurrence of DT. The molecular mechanism underlying the aggressive features of tumours in the high-risk group remains to be identified.

Among the three identified genes, *IFI6* was the only gene with a *q* value < 0.05, suggesting that this gene alone could be used to stratify the prognosis of DT. In fact, the RNA-seq analysis revealed that *IFI6* mRNA expression was a good biomarker in the high-risk patient population. Further studies that use other methods to evaluate the expression of *IFI6* or its protein product, such as immunohistochemistry, may promote the clinical application of this biomarker.

Potential limitations of this study include the following points. First, although the prognostic marker for RFS should be validated by an independent validation cohort, we could not prepare enough desmoid cases with clinical information to develop an independent validation cohort. Second, the discoveries made during our study cannot be applied in the clinical setting easily due to the complexity of the RNA-seq. Although a real-time PCR assay is easier and simpler, the expression is usually normalised to some housekeeping genes, which may affect the accuracy of the assay. Therefore, we concluded that the risk score calculated by RNA-seq is a superior maker for predicting patient prognosis. Although RNA-seq is currently under development, this study may promote its development by suggesting the clinical utility of RNA-seq in analysing desmoid tumours.

In conclusion, the discoveries made during our study can be easily applied in a clinical setting. Our data emphasise the value of gene expression profiling for the prediction of a patient's prognosis after a surgical operation. We believe that our genomic and transcriptomic analyses highlight the importance of precise tumour profiling in the provision of the best possible care to patients with DT.

#### Author contribution statement

S.K., Y.N., and H.M. conceived the project and designed the study. S.K. performed the experiments. T.U., S.K., and S.K. analysed and interpreted the data. M.H., T.S., K.I., N.N., K.O., A.K., S.I., T.O., T.Y., H.K., Y.S., H.H., T.K., T.M., Y.O., D.M., and K.M. provided administrative, technical, or material support. S.K., M.H., Y.N., and H.M. wrote and edited the manuscript with feedback from all authors.

#### Funding

This study was financially supported in part through grants from the Program for Integrated Database of Clinical and Genomic Information under Grant Number JP18kk0205003, the Project for Cancer Research And Therapeutic Evolution (P-CREATE) under the Grant Number JP19cm0106502, and for the Practical Research for Innovative Cancer Control under Grant Number JP19ck0106252 from the Japan Agency for Medical

Research, and Development (AMED). This work was also supported in part by a grant from Eisai Co., Ltd.

#### Conflict of interest statement

The authors certify that no actual or potential conflict of interest in relation to this article exists.

#### Acknowledgements

The authors would like to thank A. Maruyama for technical assistance.

#### Appendix A. Supplementary data

Supplementary data to this article can be found online at <https://doi.org/10.1016/j.ejca.2020.12.001>.

#### References

- [1] Kasper B, Strobel P, Hohenberger P. Desmoid tumors: clinical features and treatment options for advanced disease. *Oncologist* 2011;16:682–93.
- [2] Salas S, Chibon F, Noguchi T, Terrier P, Ranchere-Vince D, Lagarde P, et al. Molecular characterization by array comparative genomic hybridization and DNA sequencing of 194 desmoid tumors. *Genes Chromosomes Cancer* 2010;49:560–8.
- [3] Alman BA, Li C, Pajerski ME, Diaz-Cano S, Wolfe HJ. Increased beta-catenin protein and somatic APC mutations in sporadic aggressive fibromatoses (desmoid tumors). *Am J Pathol* 1997;151:329–34.
- [4] Trautmann M, Rehkemper J, Gevensleben H, Becker J, Wardelmann E, Hartmann W, et al. Novel pathogenic alterations in pediatric and adult desmoid-type fibromatosis - a systematic analysis of 204 cases. *Sci Rep* 2020;10:3368.
- [5] Bonvalot S, Ternes N, Fiore M, Bitsakou G, Colombo C, Honore C, et al. Spontaneous regression of primary abdominal wall desmoid tumors: more common than previously thought. *Ann Surg Oncol* 2013;20:4096–102.
- [6] Gronchi A, Casali PG, Mariani L, Lo Vullo S, Colecchia M, Lozza L, et al. Quality of surgery and outcome in extra-abdominal aggressive fibromatosis: a series of patients surgically treated at a single institution. *J Clin Oncol* 2003;21:1390–7.
- [7] Poletti JL, Williamson BD, Mitchell AW. Mammography in New Zealand: radiation dose and image quality. *Australas Phys Eng Sci Med* 1991;14:97–102.
- [8] Merchant NB, Lewis JJ, Woodruff JM, Leung DH, Brennan MF. Extremity and trunk desmoid tumors: a multifactorial analysis of outcome. *Cancer* 1999;86:2045–52.
- [9] Fiore M, Rimareix F, Mariani L, Domont J, Collini P, Le Pechoux C, et al. Desmoid-type fibromatosis: a front-line conservative approach to select patients for surgical treatment. *Ann Surg Oncol* 2009;16:2587–93.
- [10] Colombo C, Miceli R, Le Pechoux C, Palassini E, Honore C, Stacchiotti S, et al. Sporadic extra abdominal wall desmoid-type fibromatosis: surgical resection can be safely limited to a minority of patients. *Eur J Canc* 2015;51:186–92.
- [11] Klein WA, Miller HH, Anderson M, DeCosse JJ. The use of indomethacin, sulindac, and tamoxifen for the treatment of desmoid tumors associated with familial polyposis. *Cancer* 1987;60:2863–8.
- [12] Nishida Y, Tsukushi S, Shido Y, Wasa J, Ishiguro N, Yamada Y. Successful treatment with meloxicam, a cyclooxygenase-2

- inhibitor, of patients with extra-abdominal desmoid tumors: a pilot study. *J Clin Oncol* 2010;28:e107–9.
- [13] Skapek SX, Anderson JR, Hill DA, Henry D, Spunt SL, Meyer W, et al. Safety and efficacy of high-dose tamoxifen and sulindac for desmoid tumor in children: results of a Children's Oncology Group (COG) phase II study. *Pediatr Blood Canc* 2013; 60:1108–12.
  - [14] Fiore M, Colombo C, Radaelli S, Callegaro D, Palassini E, Barisella M, et al. Hormonal manipulation with toremifene in sporadic desmoid-type fibromatosis. *Eur J Canc* 2015;51:2800–7.
  - [15] Skapek SX, Ferguson WS, Granowetter L, Devidas M, Perez-Atayde AR, Dehner LP, et al. Vinblastine and methotrexate for desmoid fibromatosis in children: results of a pediatric oncology group phase II trial. *J Clin Oncol* 2007;25:501–6.
  - [16] Palassini E, Frezza AM, Mariani L, Lalli L, Colombo C, Fiore M, et al. Long-term efficacy of methotrexate plus vinblastine/vinorelbine in a large series of patients affected by desmoid-type fibromatosis. *Canc J* 2017;23:86–91.
  - [17] Chugh R, Wathen JK, Patel SR, Maki RG, Meyers PA, Schuetze SM, et al. Efficacy of imatinib in aggressive fibromatosis: results of a phase II multicenter Sarcoma Alliance for Research through Collaboration (SARC) trial. *Clin Canc Res* 2010;16:4884–91.
  - [18] Gounder MM, Mahoney MR, Van Tine BA, Ravi V, Attia S, Deshpande HA, et al. Sorafenib for advanced and refractory desmoid tumors. *N Engl J Med* 2018;379:2417–28.
  - [19] Toulmonde M, Pulido M, Ray-Coquard I, Andre T, Isambert N, Chevreau C, et al. Pazopanib or methotrexate-vinblastine combination chemotherapy in adult patients with progressive desmoid tumours (DESMOPAZ): a non-comparative, randomised, open-label, multicentre, phase 2 study. *Lancet Oncol* 2019;20:1263–72.
  - [20] Salas S, Dufresne A, Bui B, Blay JY, Terrier P, Ranchere-Vince D, et al. Prognostic factors influencing progression-free survival determined from a series of sporadic desmoid tumors: a wait-and-see policy according to tumor presentation. *J Clin Oncol* 2011;29:3553–8.
  - [21] Crago AM, Denton B, Salas S, Dufresne A, Mezhr JJ, Hameed M, et al. A prognostic nomogram for prediction of recurrence in desmoid fibromatosis. *Ann Surg* 2013;258:347–53.
  - [22] Peng PD, Hyder O, Mavros MN, Turley R, Groeschl R, Firoozmand A, et al. Management and recurrence patterns of desmoids tumors: a multi-institutional analysis of 211 patients. *Ann Surg Oncol* 2012;19:4036–42.
  - [23] Mullen JT, Delaney TF, Kobayashi WK, Szymonifka J, Yeap BY, Chen YL, et al. Desmoid tumor: analysis of prognostic factors and outcomes in a surgical series. *Ann Surg Oncol* 2012; 19:4028–35.
  - [24] Colombo C, Miceli R, Lazar AJ, Perrone F, Pollock RE, Le Cesne A, et al. CTNNB1 45F mutation is a molecular prognosticator of increased postoperative primary desmoid tumor recurrence: an independent, multicenter validation study. *Cancer* 2013;119:3696–702.
  - [25] Lazar AJ, Tuvin D, Hajibashi S, Habeeb S, Bolshakov S, Mayordomo-Aranda E, et al. Specific mutations in the beta-catenin gene (CTNNB1) correlate with local recurrence in sporadic desmoid tumors. *Am J Pathol* 2008;173:1518–27.
  - [26] Li H, Durbin R. Fast and accurate short read alignment with Burrows-Wheeler transform. *Bioinformatics* 2009;25:1754–60.
  - [27] Yoon S, Xuan Z, Makarov V, Ye K, Sebat J. Sensitive and accurate detection of copy number variants using read depth of coverage. *Genome Res* 2009;19:1586–92.
  - [28] Beroukheim R, Getz G, Nghiemphu L, Barretina J, Hsueh T, Linhart D, et al. Assessing the significance of chromosomal aberrations in cancer: methodology and application to glioma. *Proc Natl Acad Sci U S A* 2007;104:20007–12.
  - [29] Mermel CH, Schumacher SE, Hill B, Meyerson ML, Beroukheim R, Getz G. GISTIC2.0 facilitates sensitive and confident localization of the targets of focal somatic copy-number alteration in human cancers. *Genome Biol* 2011;12:R41.
  - [30] Colombo C, Urbini M, Astolfi A, Collini P, Indio V, Belfiore A, et al. Novel intra-genic large deletions of CTNNB1 gene identified in WT desmoid-type fibromatosis. *Genes Chromosomes Cancer* 2018;57:495–503.
  - [31] Suzuki A, Minamide R, Iwata J. WNT/beta-catenin signaling plays a crucial role in myoblast fusion through regulation of nephrin expression during development. *Development* 2018;145.
  - [32] Panagiotou ES, Sanjurjo Soriano C, Poulter JA, Lord EC, Dzulova D, Kondo H, et al. Defects in the cell signaling mediator beta-catenin cause the retinal vascular condition FEVR. *Am J Hum Genet* 2017;100:960–8.
  - [33] Nuytens JJ, Rust PF, Thomas Jr CR, Turrissi 3rd AT. Surgery versus radiation therapy for patients with aggressive fibromatosis or desmoid tumors: a comparative review of 22 articles. *Cancer* 2000;88:1517–23.
  - [34] Tahara Jr E, Tahara H, Kanno M, Naka K, Takeda Y, Matsuzaki T, et al. G1P3, an interferon inducible gene 6-16, is expressed in gastric cancers and inhibits mitochondrial-mediated apoptosis in gastric cancer cell line TMK-1 cell. *Cancer Immunol Immunother* 2005;54:729–40.
  - [35] Cheriya V, Glaser KB, Waring JF, Baz R, Hussein MA, Borden EC. G1P3, an IFN-induced survival factor, antagonizes TRAIL-induced apoptosis in human myeloma cells. *J Clin Invest* 2007;117:3107–17.
  - [36] Qi Y, Li Y, Zhang Y, Zhang L, Wang Z, Zhang X, et al. IFI6 inhibits apoptosis via mitochondrial-dependent pathway in dengue virus 2 infected vascular endothelial cells. *PLoS One* 2015; 10:e0132743.
  - [37] Cheriya V, Kuhns MA, Jacobs BS, Evangelista P, Elson P, Downs-Kelly E, et al. G1P3, an interferon- and estrogen-induced survival protein contributes to hyperplasia, tamoxifen resistance and poor outcomes in breast cancer. *Oncogene* 2012; 31:2222–36.
  - [38] Cheriya V, Kaur J, Davenport A, Khalel A, Chowdhury N, Gaddipati L. G1P3 (IFI6), a mitochondrial localised anti-apoptotic protein, promotes metastatic potential of breast cancer cells through mtROS. *Br J Canc* 2018;119:52–64.
  - [39] Gupta R, Forloni M, Bisserier M, Dogra SK, Yang Q, Wajapeyee N. Interferon alpha-inducible protein 6 regulates NRASQ61K-induced melanomagenesis and growth. *eLife* 2016;5.
  - [40] Liu C, Sun C, Huang H, Janda K, Edgington T. Overexpression of legumain in tumors is significant for invasion/metastasis and a candidate enzymatic target for prodrug therapy. *Canc Res* 2003; 63:2957–64.
  - [41] Haugen MH, Boye K, Nesland JM, Pettersen SJ, Egeland EV, Tamhane T, et al. High expression of the cysteine proteinase legumain in colorectal cancer - implications for therapeutic targeting. *Eur J Canc* 2015;51:9–17.
  - [42] Murthy RV, Arbman G, Gao J, Roodman GD, Sun XF. Legumain expression in relation to clinicopathologic and biological variables in colorectal cancer. *Clin Canc Res* 2005;11: 2293–9.
  - [43] Lin Y, Qiu Y, Xu C, Liu Q, Peng B, Kaufmann GF, et al. Functional role of asparaginyl endopeptidase ubiquitination by TRAF6 in tumor invasion and metastasis. *J Natl Cancer Inst* 2014;106:dju012.
  - [44] Rui M, Xia D, Zhang Y, Han W, Wang L, Ding P, et al. Molecular cloning and characterization of four isoforms of mCKLF, mouse homologues of human chemokine-like factor. *Mol Biol Rep* 2003;30:229–37.